Hydrol. Earth Syst. Sci. Discuss., 11, 4851–4878, 2014
www.hydrol-earth-syst-sci-discuss.net/11/4851/2014/
doi:10.5194/hessd-11-4851-2014

Hydrology and Earth System Sciences Discussions
Open Access

Explaining and forecasting interannual variability in the flow of the Nile River

M. S. Siam and E. A. B. Eltahir

Ralph M. Parsons Laboratory, Massachusetts Institute of Technology, Cambridge, Massachusetts, USA

Received: 1 April 2014 – Accepted: 25 April 2014 – Published: 14 May 2014

Correspondence to: M. S. Siam (msiam@mit.edu)

Published by Copernicus Publications on behalf of the European Geosciences Union.

Abstract

The natural interannual variability in the flow of Nile River had a significant impact on the ancient civilizations and cultures that flourished on the banks of the river. This is evident from stories in the Bible and Koran, and from the numerous Nilometers discovered near ancient temples. Here, we analyze extensive data sets collected during the 20th century and define four modes of natural variability in the flow of Nile River, identifying a new significant potential for improving predictability of floods and droughts. Previous studies have identified a significant teleconnection between the Nile flow and the Eastern Pacific Ocean. El Niño–Southern Oscillation (ENSO) explains about 25 % of the interannual variability in the Nile flow. Here, we identify, for the first time, a region in the southern Indian Ocean with similarly strong teleconnection to the Nile flow. Sea Surface Temperature (SST) in the region (50–80° E and 25–35° S) explains 28 % of the interannual variability in the Nile flow. During those years with anomalous SST conditions in both Oceans, we estimate that indices of the SSTs in the Pacific and Indian Oceans can collectively explain up to 84 % of the interannual variability in the flow of Nile. Building on these findings, we use classical Bayesian theorem to develop a new hybrid forecasting algorithm that predicts the Nile flow based on global models predictions of indices of the SST in the Eastern Pacific and Southern Indian Oceans.

1 Introduction

The Nile basin covers an area of 2.9×10^6 km^2, which is approximately 10 % of the African continent (Fig. 1). It has two main tributaries; the White Nile and the Blue Nile that originate from the equatorial lakes and Ethiopian highlands respectively. The Upper Blue Nile (UBN) basin is the main source of water for the Nile River. It contributes to approximately 60 % of the annual flow of the Nile and 80 % of the total Nile flow that occurs between July and October at Dongola (Conway and Hulme, 1993) (Fig. 2). The UBN basin extends over an area of 175×10^3 km^2 (7° N to 12°5′ N and from 34°5′ E

HESSD
11, 4851–4878, 2014

Explaining interannual variability in the Nile River flow

M. S. Siam and E. A. B. Eltahir

to 40° E). The mean annual rainfall over this basin is 1200 mm $year^{-1}$ (Conway and Hulme, 1993). Almost 60 % of the annual rainfall over the UBN occurs during the summer between July and August, resulting in a largely predictable seasonal variability in the flow of the river.

The predictability of inter-annual variability in the flow of the Nile is rather challenging. A significant fraction of this variability is shaped by El Niño–Southern Oscillation (ENSO) (Eltahir, 1996; Abtew et al., 2009; and Melesse et al., 2011). The SSTs anomalies over the tropical Eastern Pacific Ocean explains 25 % of the inter-annual variability of Nile flow (Eltahir, 1996). This high correlation was the basis for new forecast models that were proposed to predict the Nile flows. Wang and Eltahir (1999) used a discriminant prediction approach to estimate the probabilities that the Nile flow will fall into prescribed categories. Eldaw et al. (2003) used sea surface temperature (SST) over 22 regions in the Pacific, Indian and Atlantic Oceans as predictors within a multiple linear regression model to predict the Nile flow.

The connection between El Niño events and the rainfall over Eastern Africa was investigated in several studies (e.g., Beltrando and Camperlin, 1993). However, a clear distinction must be made between rainfall over the UBN basin and rainfall over East Africa, defined as the region along the coast, east of the Ethiopian highlands (Fig. 1). The mechanism that connects rainfall over these regions to ENSO is different from the mechanism that connects ENSO to rainfall over the UBN basin. The UBN basin has one rainy season (May to September) during which more than 80 % of the rainfall occurs, while along the East coast of Africa and depending on the location from the equator, the seasonal cycle of rainfall can have two rainy seasons (Black et al., 2003; Hastenrath et al., 2011). This pattern in the seasonal cycle of rainfall is related to the migration of the Inter-tropical Convergence Zone (ITCZ) across the equator. The warm phase of ENSO is positively correlated with the short rainy season (October to December) over East Africa. However, the rainfall during the long rainy season (March to June) is not correlated to ENSO (Mutai and Neil, 2000; Pohl and Camberlin, 2006). In contrast,

HESSD
11, 4851–4878, 2014

the rainfall over the UBN basin (May to September), is negatively correlated to ENSO (Amarasekera et al., 1996).

Rainfall over East Africa, including the UBN basin, is strongly coupled with the dynamics of the Indian monsoon (Camberlin, 1995). During strong Indian monsoon seasons, the sea level pressure over India decreases significantly, which enhances the pressure gradient between East Africa and India. As a result, westerly winds increase over Eastern Africa, which advect moisture from the Congo basin to Ethiopia, Uganda and western Kenya (Camberlin, 1995). During El Niño events, the monsoon circulation is weaker due to modulation of the walker circulation and enhanced subsidence over the Western Pacific and South Asia (Ju and Slingo, 1995; Kawamura, 1998; Shukla and Wallace, 1983; Soman and Slingo, 1997). The reduced Nile flows during El Niño events were also attributed to the enhanced tropical-scale subsidence that suppresses rainfall, as a consequence of the increased upwelling over the Eastern Pacific Ocean (Amarasekera et al., 1996).

The connection between SSTs of North and Middle Indian Ocean and Nile flow is strongly modulated by ENSO through ocean currents. During El Niño events, the warm water travels from the Pacific to the Indian Ocean through the “Indonesian through flow” and advection by the Indian Equatorial Current (Tomczak and Godfrey, 1995). As a result, SSTs in North and Middle Indian Ocean warm-up following the warming of Tropical Eastern Pacific, and forces a Gill type circulation anomaly with enhanced westerly winds over Western Indian Ocean (Yang et al., 2007). The latter enhances the low-level divergence of air and moisture away from the Upper Blue Nile resulting in a reduction of rainfall over the basin (Siam et al., 2014). In comparison the Southern Indian Ocean is not impacted significantly by ocean currents from the Pacific Ocean.

In this paper, we propose that SST in the Southern region of Indian Ocean plays a significant role in shaping the variability of Nile flow that is independent from ENSO. The physical mechanism for this tele-connection is described in another paper by the authors (Siam et al., 2014). The warming over the South IO, generates a cyclonic flow in the boundary layer, which reduces the cross-equatorial meridional transport of air

HESSD
11, 4851–4878, 2014

and moisture towards the UBN basin, favoring a reduction in rainfall and river flow. The tele-connections between the Pacific Ocean and the Nile basin and between the Indian Ocean and the Nile basin are reflected in different modes of observed natural variability in the flow of Nile River, with important implications for the predictability of floods and droughts.

The objectives of the study are (i) to investigate the teleconnection between the Indian Ocean and the Nile basin and its role in explaining observed natural variability in the flow of the Nile River, and (ii) to develop a new hybrid forecasting algorithm that can be used to predict the Nile flow based on indices of the SST in the Eastern Pacific and Southern Indian Oceans.

2 Data

In this study we use observed SSTs over the Indian and Pacific oceans from the monthly global (HadISST V1.1) dataset on a 1° latitude-longitude grid from 1900 to 2000 (Rayner et al., 2003). The monthly flows at Dongola from 1900 to 2000 were extracted from the Global River Discharge Database (RivDIS v1.1) (Vörösmarty et al., 1998). The average monthly anomalies from September to November of the SSTs averaged over the Eastern Pacific Ocean (6–2° N, 170–90° W; 2° N–6° S, 180–90° W; and 6–10° S, 150–110° W) are used as an index of ENSO. This area has shown the highest correlation with the Nile flows and it is almost covering the same area as Niño 3 and 3.4 indices (Trenberth, 1997).

3 Relation between the variability in the flow of Nile River, ENSO and the Indian Ocean SST

Based on extensive correlation analysis of the Nile River flow at Dongola and the observed SST in the Indian Ocean, we identify a region over the Southern Indian Ocean (50–80° E and 25–35° S) (see Fig. 3) as the one with the highest correlation between

HESSD
11, 4851–4878, 2014

SST and the Nile flow. This correlation is especially high for river flow (accumulated for July, August, September and October) and SST during the month of August. We introduce a new index defined as the average SST over this region of the Southern Indian Ocean (SIO index hereinafter) during the month of August. In comparison to earlier studies, ElDaw et al. (2003) used SST indices over the Indian Ocean to predict the Nile flow, however, they focused on regions of the Indian Ocean that are different from the region that we use in defining the SIO index. In other words the region of the SIO was not used by ElDaw et al. (2003). Table 2 describes the regions of the Indian Ocean identified in both studies.

Here, we emphasize that the proposed forecasting methodology for the Nile flow is motivated by the physical mechanisms proposed by Siam et al. (2014) and described in Sect. 1. However, the forecasting approach of some of the previous studies was based on purely statistical correlations found between the Nile flow and SSTs globally.

The North and middle of the Indian Ocean have also exhibited a high correlation between their SST and the Nile flow. However, the additional variability explained by the SST over the North and Middle Indian Ocean, when combined with the ENSO index, is negligible (not shown here). On the other hand, the addition of the SIO index to ENSO index enhances the explained variability in the flow of Nile River (Table 1).

In further analysis, we use a multiple linear regression model to describe the Nile flow (predictand) using indices of the SSTs over the Eastern Pacific and Indian oceans (predictors). These indices include SIO index and the ENSO index, defined for the regions shown in Fig. 3. We define 0.5 °C as the threshold between non-neutral and neutral years based on ENSO index. This value is about two-thirds of one standard deviation of the anomalies of ENSO index. The same threshold has been used to identify non-neutral and neutral years using El Niño 3.4 index, which is similar to our ENSO index (Trenberth, 1997). Similarly, 0.3 °C value is used as a threshold between non-neutral and neutral years in the SIO index. This value is about two-thirds of one standard deviation for the anomalies of the SST over this region.

Four different modes are identified for describing the natural variability in the flow of Nile River and summarized in (Table 1). The ENSO and SIO indices do not explain a significant fraction of the interannual variability in the flow of river when they are both neutral (Fig. 4a). The variability of the Nile flow in such years can be regarded as a reflection of the chaotic interactions between the biosphere and atmosphere and within each of the two domains. For this mode, the predictability of the Nile flow is rather limited. The other two intermediate modes include non-neutral conditions in the Eastern Pacific and neutral conditions in the Southern Indian Oceans or vice versa (Fig. 4b and c). For these two modes, a significant fraction (i.e., 31 and 43 %) of the variance describing inter-annual variability in the flow is explained. Hence, these modes point to a significant potential for predictability of the flow. Finally, indices of ENSO and SIO can explain 84 % of the interannual variability in the Nile flow when non-neutral conditions are observed for both the Eastern Pacific and Southern Indian Oceans (Fig. 4d). Therefore, the SIO index can be used to predict the flow together with the ENSO index, as collectively they can explain a significant fraction of the variability in the flow of Nile River. This result indicates that during years with anomalous SST conditions in both oceans, floods and droughts in the Nile River flow can be highly predictable, assuming accurate forecasts of those indices are available.

4 A hybrid methodology for long-range prediction of the Nile flow

A simple methodology is proposed to predict the Nile flow with a lead time of about a few months (~ 3–6 months). The forecast of global SST distribution based on dynamical models (e.g., NCEP coupled forecast system model version 2 (CFSv2), Saha et al., 2010, 2014), can be used together with algorithm developed in this section to relate the Nile flow to ENSO and SIO indices. The proposed method is shown in Fig. 5 and can be described in two main steps:

HESSD
11, 4851–4878, 2014

M. S. Siam and E. A. B. Eltahir

– Forecast of SST anomalies in the Indian Ocean and Eastern Pacific Ocean using dynamical models of the coupled global ocean atmosphere system. Such forecasts are routinely issued by centers such NCEP and ECMWF.

– Application of a forecast algorithm between the Nile flow (predictand) and forecasted SSTs in the Indian and Eastern Pacific Oceans (predictors) for the identified mode of variability.

In this paper we focus on the second step of the proposed method: the development of the algorithm relating SSTs and the Nile flow. We develop the forecast algorithm using observed SSTs. We do not describe how this algorithm can be applied with forecasts of global SST distribution based on dynamical models as this step is beyond the scope of this paper. However, we recognize that overall accuracy of this method in predicting interannual variability of the Nile flow is dependent on the skill of global coupled models in forecasting the global SSTs (see Appendix for information about forecasting models). Thus, the selection of the forecast model, which predicts the SSTs is an important step to ensure the accuracy of the prediction of the Nile flow. As global coupled ocean–atmosphere models improve in their skill of forecasting global SSTs in the Pacific and Indian Oceans, we expect that our ability to predict the interannual variability in the Nile flow will improve too. In addition, the accuracy in the prediction of the Nile flow at medium and short time scales (of weeks to one month) can be improved by adding other hydrological variables (e.g., rainfall and stream flow) over the basin, as demonstrated by Wang and Eltahir (1999).

The proposed method can be described as hybrid since it combines dynamical forecasts of global SSTs, and statistical algorithms relating the Nile flow and the forecasted SSTs. The same method can also be described as hybrid since it combines information about SSTs from the Pacific and the Indian Oceans.

Here, we apply a discriminant approach that specifies the categoric probabilities of the predictand (Nile flow) according to the categories that the predictors (i.e., ENSO and SIO indices) fall into. The annual Nile flow is divided into "low", "normal", and

HESSD
11, 4851–4878, 2014

"high" categories. The boundaries of these categories are defined so that the number of points in each category is about a third of the data points (Fig. 6). On the other hand, the ENSO and SIO indices are divided into "cold", "normal" and "warm" categories. (The words Normal and Neutral are used to describe the same conditions.) The boundaries for the normal category are −0.5 and 0.5 °C for ENSO index and −0.3 and 0.3 °C for SIO index (Fig. 6). Any condition below the lower limit is considered "cold" and higher than the upper limit is considered "warm" for both indices.

The Bayesian theorem, described in many statistical books (e.g., Winkler, 1972; West, 1989), states that the probability of occurrence of a specified flow category (Q_i) and given two conditions (A and B) can be expressed as

$$P(Q_i/\mathrm{A},\mathrm{B}) = \frac{P(\mathrm{B}/Q_i,\mathrm{A})P(Q_i/\mathrm{A})}{P(\mathrm{B}/\mathrm{A})} \tag{1}$$

where $P(Q_i/\mathrm{A})$ is the probability of event Q_i given that event A has occurred, and $P(Q_i/\mathrm{A},\mathrm{B})$ is the probability of event Q_i given that events A and B have occurred, and similarly for other shown probabilities. In addition, if the events A and B are independent, we can rewrite Eq. (1) as

$$P(Q_i/\mathrm{A},\mathrm{B}) = \frac{P(\mathrm{B}/Q_i)P(Q_i/\mathrm{A})}{\sum_{i=1}^{3} P(\mathrm{B}/Q_i)P(Q_i/\mathrm{A})}. \tag{2}$$

The advantage of assuming independence between (A and B) and using Eq. (2), it simplifies the calculation of $P(\mathrm{B}/Q_i,\mathrm{A})$ since we do not have to split the data into a relatively large number of categories, which reduces the error due to the limitation of the data size. The independence between ENSO and SIO indices is a reasonable assumption as the coefficient of determination between them is less than 6 %.

HESSD
11, 4851–4878, 2014

In order to evaluate the predictions of the Nile flow, we use a forecasting index (FI) defined by Wang and Eltahir (1999) as

$$\mathrm{FP}(j) = \sum_{i=1}^{3} P_\mathrm{r}(i,j)P_\mathrm{p}(i,j) \tag{3}$$

$$\mathrm{FI} = \frac{1}{n}\sum_{i=1}^{n} \mathrm{FP}(j) \tag{4}$$

where FP(j) is the forecast probability in a certain year (j) and the FI is the average of the FP over a certain period, n. The prior probability $P_\mathrm{r}(i,j)$ is calculated using Eq. (2) for a certain year (j) and category ($i = 1,2,3$) and the posterior probability $P_\mathrm{p}(i,j)$ is defined as [1,0,0] in low flow year, [0,1,0] in normal year, and [0,0,1] in a high flow year. Hence, a larger FI indicates a higher accuracy of the forecast. The FI without any information about SST, should be about one third as we have classified flow data into three categories each with a similar number of the data points.

The data is split into a calibration period (1900–1970) and a verification period (1970–2000). Tables 3 and 4 summarize the conditional probabilities of Nile flow given certain conditions of SIO or ENSO index. It is shown that during "warm" and "cold" conditions of SIO, the probabilities are significantly higher for "low" and "high" Nile flow, respectively. The same is true for the ENSO, as was described originally by Eltahir (1996). Table 5 shows the probabilities that are conditioned on both SIO and ENSO, calculated using Eq. (2). This table illustrates clearly how forecasts of the Nile flow can be improved by combining the two indices. For example, "warm" conditions in both oceans translate into 85 % probability of "low" flow in the Nile, and insignificant probability of "high" flow. On the other hand, "cold" conditions in both oceans translate into 83 % probability of "high" flow in the Nile, and insignificant probability of "low" flow. Depending on the accuracy of the dynamical forecast models of global SSTs, such forecast of the Nile flow can be issued with lead times of 6 months. At present, the Eastern Nile Regional technical Office (ENTRO) issues operational forecasts of the Nile flow based on ENSO forecasts and the probability table described by Eltahir (1996) (similar to Table 4). We anticipate that use of Table 5, would represent a significant improvement in these operational forecasts.

The combined use of ENSO and the SIO indices significantly increased the FI to 0.5 (Fig. 7a). Comparison of Fig. 6b and c illustrates that the SIO index alone has almost the same FI value as ENSO index. Recall that in absence of any information about global SSTs, the FI should have a value of one third. The deviations of the FI using ENSO index alone (Fig. 7b) or SIO index alone (Fig. 7c) from one third are almost added together to create the deviation of the FI from the hybrid method from one third (Fig. 7a). Hence, the new SIO index plays an independent role from ENSO in shaping the interannual variability in the flow of Nile River. Thus by using these two indices, we explain a significant fraction of the interannual variability in the flow of Nile River, and illustrate a significant potential for improving the Nile flow forecasts.

5 Conclusions

- In this paper, we document that the SSTs in the Eastern Pacific and Indian Oceans play a significant role in shaping the natural interannual variability in the flow of Nile River. Previous studies have identified a significant teleconnection between the Nile flow and the Eastern Pacific Ocean. El Niño–Southern Oscillation (ENSO) explains about 25 % of the interannual variability in the Nile flow. Here, we identify, for the first time, a region in the southern Indian Ocean with similarly strong teleconnection to the Nile flow. Sea Surface Temperature (SST) in the region (50–80° E and 25–35° S) explains 28 % of the interannual variability in the Nile flow.

- In addition, four different modes of natural variability in the Nile flow are identified and it is shown that during non-neutral conditions in both the Pacific and Indian Oceans, the Nile flow is highly predictable using global SST information. During

HESSD
11, 4851–4878, 2014

M. S. Siam and E. A. B. Eltahir

those years with anomalous SST conditions in both Oceans, we estimate that indices of the SSTs in the Pacific and Indian Oceans can collectively explain up to 84 % of the interannual variability in the flow of Nile. The estimated relationships between the Nile flow and these indices allow for accurately predicting the Nile floods and droughts using observed or forecasted conditions of the SSTs in the two oceans.

– We use classical Bayesian theorem to develop a new hybrid forecasting algorithm that predicts the Nile flow based on indices of the SST in the Eastern Pacific and Southern Indian Oceans. "Warm" conditions in both oceans translate into 85 % probability of "low" flow in the Nile, and insignificant probability of "high" flow. On the other hand, "cold" conditions in both oceans translate into 83 % probability of "high" flow in the Nile, and insignificant probability of "low" flow. Applications of the proposed hybrid forecast method should improve predictions of the interannual variability in the Nile flow, adding a new a tool for better management of the water resources of the Nile basin.

The proposed forecasting methodology is indeed dependent on the accuracy of the global SST forecasts from global dynamical models. The accuracy of these forecasts is likely to improve as the models are tested and developed further. However, in this paper we test the proposed forecasting algorithm using observed SSTs. Such test describes an upper limit of the skill of the proposed algorithm. The assessment of the same methodology using indices of SST forecasted by global dynamical models will be addressed in future work.

References

Abtew, W., Melesse, A. M., and Dessalegne, T.: El Niño Southern Oscillation link to the Blue Nile River Basin hydrology, Hydrol. Process., 23, 3653–3660, doi:10.1002/hyp.7367, 2009.

Amarasekera, K. N., Lee, R. F., Williams, E. R., and Eltahir, E. A. B.: ENSO and the natural variability in the flow of tropical rivers, J. Hydrol., 200, 24–39, 1996.

HESSD

11, 4851–4878, 2014

Explaining interannual variability in the Nile River flow

M. S. Siam and E. A. B. Eltahir

Bacmeister, J., Pegion, P. J., Schubert, S. D., and Suarez, M. J.: An atlas of seasonal means simulated by the NSIPP 1 atmospheric GCM, Vol. 17, NASA Tech. Memo. 104606, Goddard Space Flight Center, Greenbelt, MD, 194 pp., 2000.
Beltrando, G. and Camberlin, P.: Interannual variability of rainfall in Eastern Horn of Africa and indicators of atmospheric circulation, Int. J. Climatol., 13, 533–546, 1993.
Black, E., Slingo, J., and Sperber, K. R.: An observational study of the relationship between excessively strong short rains in coastal East Africa and Indian Ocean SS T, Mon. Weather Rev., 31, 74–94, 2003.
Camberlin, P.: June–September rainfall in North-Eastern Africa and atmospheric signals over the tropics: a zonal perspective, Int. J. Climatol., 15, 773–783, 1995.
Camberlin, P.: Rainfall anomalies in the source region of the Nile and their connection with the Indian summer monsoon, J. Climate, 10, 1380–1392, 1997.
Conway, D. and Hulme, M.: Recent Fluctuations in precipitation and runoff over the Nile sub-basins and their impact on Main Nile discharge, Climatic Change, 25, 127–151, 1993.
ElDaw, A., Salas, J. D., and Garcia, L. A.: Long range forecasting of the Nile River flows using climate forcing, J. Appl. Meteorol., 42, 890–904, 2003.
Eltahir, E. A. B.: El Nino and the natural variability in the flow of the Nile River, Water Resour. Res., 32, 131–137, 1996.
Graham. R., Gordon, M., McLean, P. J., Ineson, S., Huddleston, M. R., Davey, M. K., Brookshaw, A., and Barnes, R. T. H.: A performance comparison of coupled and uncoupled versions of the Met Office seasonal prediction general circulation model, Tellus A, 57, 320–339, 2005.
Hastenrath, S., Polzin, D., and Mutai, C.: Circulation mechanisms of Kenya rainfall anomalies, J. Climate, 24, 404–412, 2011.
Ju, J. and Slingo, J. M.: The Asian summer monsoon and ENSO, Q. J. Roy. Meteorol. Soc., 121, 1133–1168, 1995.
Kawamura, R.: A possible mechanism of the Asian summer monsoon-ENSO coupling, J. Meteorol. Soc. Jpn., 76, 1009–1027, 1998.
Melesse, A., Abtew, W., Setegn, S. G., and Desalegn, T.:. Hydrological Variability and Climate of the Upper Blue Nile River Basin, in: Nile River Basin: Hydrology, Climate and Water Use, 1st Edn., edited by: Melesse, A. M., Springer, 2011, p. 480, 200 illus, Part 1, 3–37, doi:10.1007/978-94-007-0689-7_1, 2011.

HESSD
11, 4851–4878, 2014

Molteni, F., Stockdale, T., Balmaseda, M., Balsamo, G., Buizza, R., Ferranti, L., Magnusson, L., Mogensen, K., Palmer, T., and Vitart, F.: The new ECMWF seasonal forecast system (System 4), ECMWF Research Department Technical Memorandum n. 656, ECMWF, Shinfield Park, Reading, UK, 51 pp., 2011.
Mutai, C. C. and Ward, M. N.: East African rainfall and the tropical circulation/convection on intraseasonal to interannual timescales, J. Climate, 13, 3915–3939, 2000.
Penland, C. and Matrosova, L.: Prediction of tropical Atlantic Sea surface temperatures using linear inverse modeling, J. Climate, 11, 483–496, 1998.
Pohl, B. and Camberlin, P.: Influence of the Madden-Julian Oscillation on East African rainfall, Part I: Intraseasonal variability and regional dependency, Q. J. Roy. Meteorol. Soc., 132, 2521–2539, 2006.
Saha, S., Moorthi, S., Pan, H.-L., Wu, X., Wang, J., Nadiga, S., Tripp, P., Kistler, R., Woollen, J., Behringer, D., Liu, H., Stokes, D., Grumbine, R., Gayno, G., Hou, Y.-T., Chuang, H.-Y., Juang, H.-M. H., Sela, J., Iredell, M., Treadon, R., Kleist, D., van Delst, P., Keyser, D., Derber, J., Ek, M., Meng, J., Wei, H., Yang, R., Lord, S., van den Dool, H., Kumar, A., Wang, W., Long, C., Chelliah, M., Xue, Y., Huang, B., Schemm, J.-K., Ebisuzaki, W., Lin, R., Xie, P., Chen, M., Zhou, S., Higgins, W., Zou, C.-Z., Liu, Q., Chen, Y., Han, Y., Cucurull, L., Reynolds, R. W., Rutledge, G., and Goldberg, M.: The NCEP Climate Forecast System Reanalysis, B. Am. Meteorol. Soc., 91, 1015–1057, doi:10.1175/2010BAMS3001.1, 2010.
Saha, S., Moorthi, S., Wu, X., Wang, J., Nadiga, S., Tripp, P., Pan, H.-L., Behringer, D., Hou, Y.-T., Chuang, H.-Y., Iredell, M., Ek, M., Meng, J., Yang, R., van den Dool, H., Zhang, Q., Wang, W., and Chen, M.: The NCEP climate forecast system version 2, J. Climate, in press, 2013.
Shukla, J. and Wallace, J. M.: Numerical simulation of the atmospheric response to equatorial Pacific sea surface temperature anomalies, J. Atmos. Sci., 40, 1613–1630,1983.
Siam, M. S., Wang, G., Estelle, M. E., and Eltahir, E. A. B.: Role of the Indian Ocean Sea surface temperature in shaping natural variability in the flow of the Nile River, Clim. Dynam., doi:10.1007/s00382-014-2132-6, in press, 2014.
Soman, M. K. and Slingo, J.: Sensitivity of the Asian summer monsoon to aspects of sea-surface-temperature anomalies in the tropical pacific ocean, Q. J. Roy. Meteorol. Soc., 123, 309–336, 1997.
Trenberth, K. E.: The definition of El Niño, B. Am. Meteorol. Soc., 78, 2771–2777, 1997.

HESSD
11, 4851–4878, 2014

Explaining interannual variability in the Nile River flow

M. S. Siam and
E. A. B. Eltahir

Wang, G. and Eltahir, E. A. B.: Use of ENSO information in medium and long range forecasting of the Nile floods, J. Climate, 12, 1726–1737, 1999.
West, M.: Bayesian Forecasting and Dynamic Models, Springer, New York, 704 pp., 1989.
Winkler, P. B.: Homogenized long-period Southern Oscillation indices, Int. J. Climatol., 9, 33–54, 1989.
Xue, Y., Leetmaa, A., and Ji, M.: ENSO prediction with Markov model: the impact of sea level, J. Climate, 13, 849–871, 2000.
Yang, J. L., Liu, Q. Y., Xie, S. P., Liu, Z., and Wu, L.: Impact of the Indian Ocean SST basin mode on the Asian summer monsoon, Geophys. Res. Lett., 34, L02708, doi:10.1029/2006GL028571, 2007.

HESSD
11, 4851–4878, 2014

Explaining interannual variability in the Nile River flow

M. S. Siam and E. A. B. Eltahir

Table 1. Summary of the coefficient of determination (R^2) between the average Nile flow from July to October and different combination of indices of ENSO and SIO.

Mode ENSO	SIO	ENSO	SIO	ENSO, SIO	Number of events (Observed Variance of Nile flow)
Neutral	Neutral	0.04	0.03	0.08	29 (6.76)
Neutral	Non-Neutral	0.05	0.28*	0.31*	26 (10.24)
Non-Neutral	Neutral	0.4*	0.02	0.43*	26 (5.8)
Non-Neutral	Non-Neutral	0.64*	0.6*	0.84*	19 (12.3)

SIO: South Indian Ocean SSTs index, ENSO: ENSO index.
* Values that are significant at 1 % significance level.

HESSD
11, 4851–4878, 2014

Explaining interannual variability in the Nile River flow

M. S. Siam and E. A. B. Eltahir

Table 2. Comparison between regions in the Indian Ocean used in ElDaw et al., 2003 and this study to predict the Nile flow.

Region	Location	Study
1	(35–44° S, 115–130° E)	ElDaw et al. (2003)
2	(0–7° S, 90–130° E)	
3	(35–44° S, 20–60° E)	
4	(10–20° S, 110–125° E)	
5	(50–80° E and 25–35° S)	This study

HESSD
11, 4851–4878, 2014

M. S. Siam and E. A. B. Eltahir

Table 3. Conditional probability of the Nile flow given SIO conditions.

		Nile flow		
		High	Normal	Low
SIO	Warm	0	0.25	0.75
	Normal	0.23	0.39	0.39
	Cold	0.57	0.26	0.17

HESSD

11, 4851–4878, 2014

Table 4. Conditional probability of the Nile flow given ENSO conditions.

		Nile flow		
		High	Normal	Low
ENSO	Warm	0.15	0.31	0.54
	Normal	0.22	0.38	0.41
	Cold	0.68	0.32	0

HESSD
11, 4851–4878, 2014

M. S. Siam and
E. A. B. Eltahir

Table 5. Conditional probability of the Nile flow given SIO and ENSO conditions.

SIO	Nile flow	ENSO		
		Warm	Normal	Cold
SIO Warm	High	0	0	0
	Normal	0.15	0.22	1
	Low	0.85	0.78	0
SIO Normal	High	0.1	0.14	0.57
	Normal	0.31	0.4	0.43
	Low	0.59	0.46	0
SIO Cold	High	0.33	0.42	0.83
	Normal	0.29	0.33	0.17
	Low	0.37	0.25	0

HESSD
11, 4851–4878, 2014

Table A1. Summary of some available forecast models of the Sea Surface Temperature.

Model	Type of Model	Agency	Domain	Lead time up to (Months)	Resolution (km)	Reference
NCEP-CFS V2	Dynamical	National Centers for Environmental Prediction (NCEP)	Global	8	200	Saha et al. (2010)
NASA-GMAO	Dynamical	NASA Goddard Space Flight Center – Global Modeling and Assimilation Office	Global	12	200	Bacmeister et al. (2000)
ECMWF-System 4	Dynamical	European Centre for Medium-Range Weather Forecasts	Global	4	70	Molteni et al. (2011)
UKMO-GCM	Dynamical	UK Met Office	Global	6	150	Graham et al. (2005)
NOAA-CDC	Statistical	National Oceanic and Atmospheric Administration – Climate Diagnostic Center	Global	12	–	Pneland et al. (1998)
CPC-Markov	Statistical	National Centers for Environmental Prediction – Climate Prediction Center	Nino 3 and Nino 3.4	8	–	Xue et al. (2000)

HESSD
11, 4851–4878, 2014

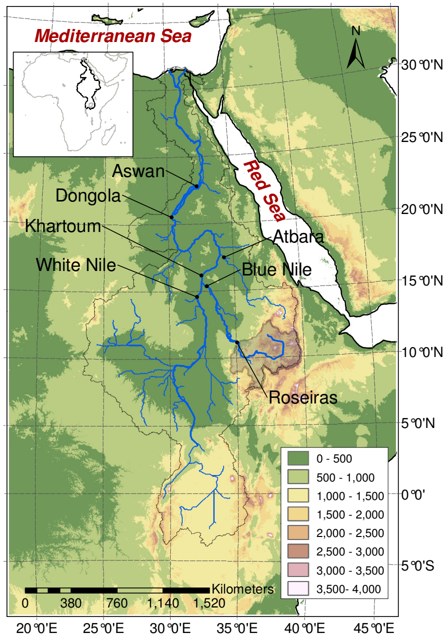

Fig. 1. Topographic map of the Nile basin showing the outlet of the Upper Blue Nile basin (shaded in gray) at Roseiras. The White and Blue Nile join together at Khartoum the form the main branch of the Nile that flows directly to Dongola in the North.

HESSD
11, 4851–4878, 2014

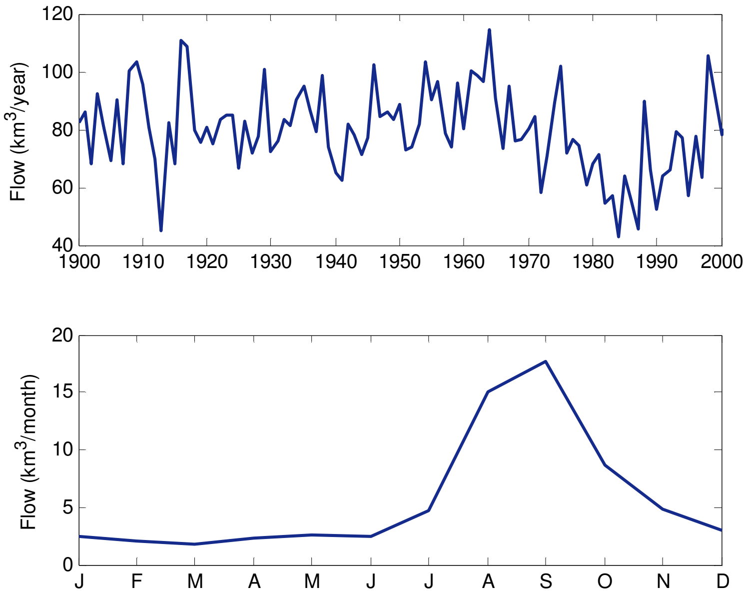

Fig. 2. Annual Nile flow (top panel) and seasonal cycle (bottom panel) of the flow at Dongola for the period from 1900 to 2000.

HESSD
11, 4851–4878, 2014

Explaining interannual variability in the Nile River flow

M. S. Siam and E. A. B. Eltahir

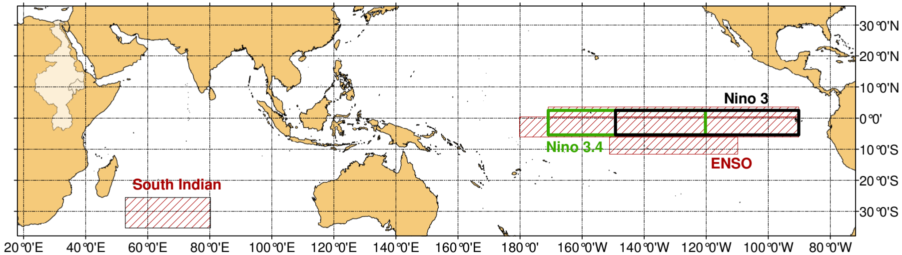

Fig. 3. World map showing areas that cover the ENSO and North and South Indian Ocean SSTs indices. The Nino 3 and 3.4 are outlined in blue and green respectively. The whole Nile basin is outlined in black.

HESSD
11, 4851–4878, 2014

Explaining interannual variability in the Nile River flow

M. S. Siam and E. A. B. Eltahir

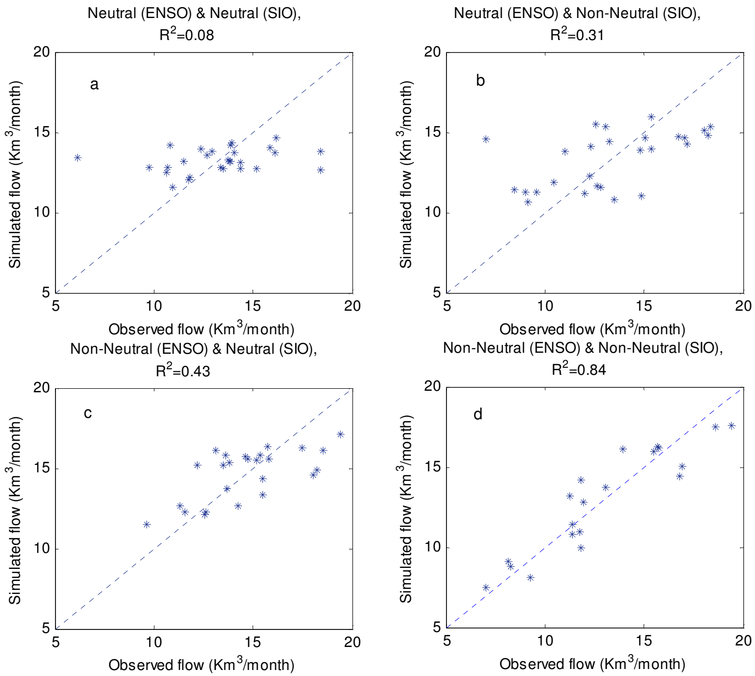

Fig. 4. A comparison between the observed and simulated Nile flow showing the different modes of variability for the period from 1900 to 2000: **(a)** Neutral ENSO and SIO, **(b)** Neutral ENSO and Non-Neutral SSTs in SIO, **(c)** Non-Neutral ENSO and Neutral SSTs in SIO and finally, **(d)** Non-Neutral ENSO and Non-Neutral SSTs in SIO.

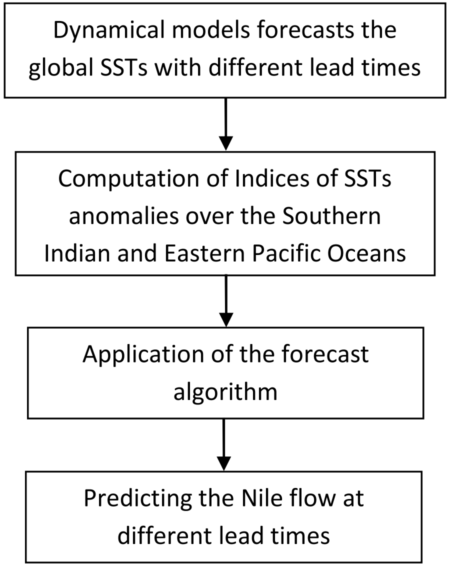

Fig. 5. Schematic of the hybrid methodology for predicting the Nile flow using the SSTs forecasts of the dynamical models and the proposed forecast algorithm.

HESSD
11, 4851–4878, 2014

Explaining interannual variability in the Nile River flow

M. S. Siam and E. A. B. Eltahir

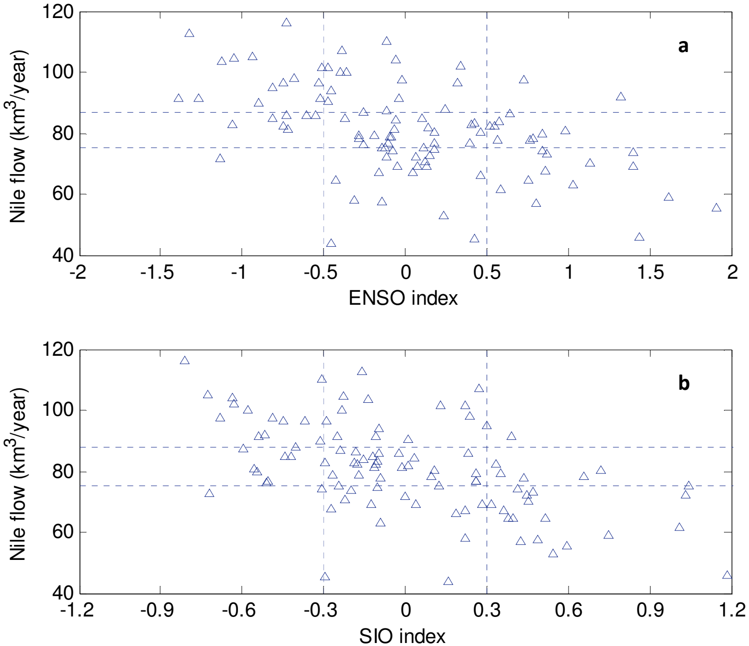

Fig. 6. Relations between the annual Nile flow and different indices for the period (1900–2000): **(a)** ENSO, and **(b)** SIO. The horizontal lines represent the boundaries for the "high", "normal" and "low" categories of the annual flow. The vertical lines represent the boundaries for the "warm", "normal", and "cold" conditions for ENSO and SIO indices.

HESSD
11, 4851–4878, 2014

Explaining interannual variability in the Nile River flow

M. S. Siam and E. A. B. Eltahir

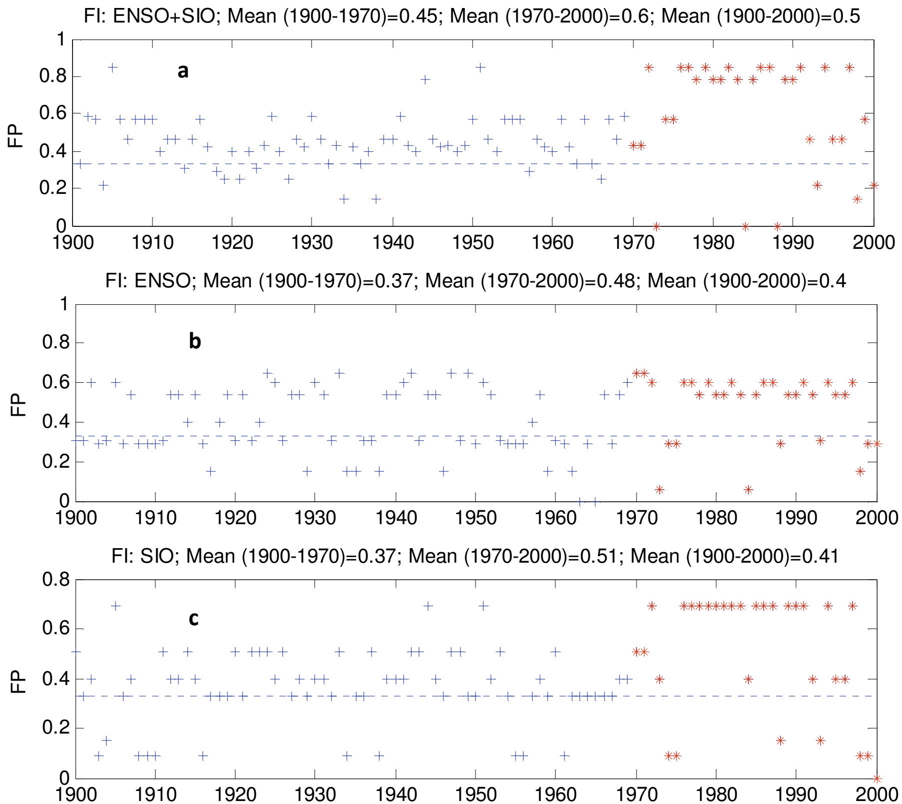

Fig. 7. Time series of the forecast probability using different indices: **(a)** ENSO and SIO together, **(b)** ENSO, and **(c)** SIO. The period (1900–1970) is used for calculating the probabilities (shown in crosses) using Eq. (2) and (1970–2000) for validation (shown in stars).